

ELP3 Controls Active Zone Morphology by Acetylating the ELKS Family Member Bruchpilot

Katarzyna Miśkiewicz,^{1,2} Liya E. Jose,^{1,2} André Bento-Abreu,^{3,4,8} Marcus Fislage,^{5,6,8} Ines Taes,^{3,4} Jarosław Kasproicz,^{1,2} Jef Swerts,^{1,2} Stephan Sigrist,⁷ Wim Versées,^{5,6} Wim Robberecht,^{3,4} and Patrik Verstreken^{1,2,*}

¹VIB, Department of Molecular and Developmental Genetics, B3000 Leuven, Belgium

²K.U.Leuven, Center for Human Genetics, B3000 Leuven, Belgium

³VIB, Vesalius Research Center, B3000 Leuven, Belgium

⁴K.U.Leuven, Laboratory for Neurobiology, Experimental Neurology, B3000 Leuven, Belgium

⁵VIB, Department of Molecular and Cellular Interactions, K.U.Leuven, B1050 Brussels, Belgium

⁶Vrije Universiteit Brussel, Structural Biology Brussels, B1050 Brussels, Belgium

⁷Freie Universität Berlin, Department of Genetics, Institute for Biology, 14195 Berlin, Germany

⁸These authors contributed equally to this work

*Correspondence: patrik.verstreken@cme.vib-kuleuven.be

DOI 10.1016/j.neuron.2011.10.010

SUMMARY

Elongator protein 3 (ELP3) acetylates histones in the nucleus but also plays a role in the cytoplasm. Here, we report that in *Drosophila* neurons, ELP3 is necessary and sufficient to acetylate the ELKS family member Bruchpilot, an integral component of the presynaptic density where neurotransmitters are released. We find that in *elp3* mutants, presynaptic densities assemble normally, but they show morphological defects such that their cytoplasmic extensions cover a larger area, resulting in increased vesicle tethering as well as a more proficient neurotransmitter release. We propose a model where ELP3-dependent acetylation of Bruchpilot at synapses regulates the structure of individual presynaptic densities and neurotransmitter release efficiency.

INTRODUCTION

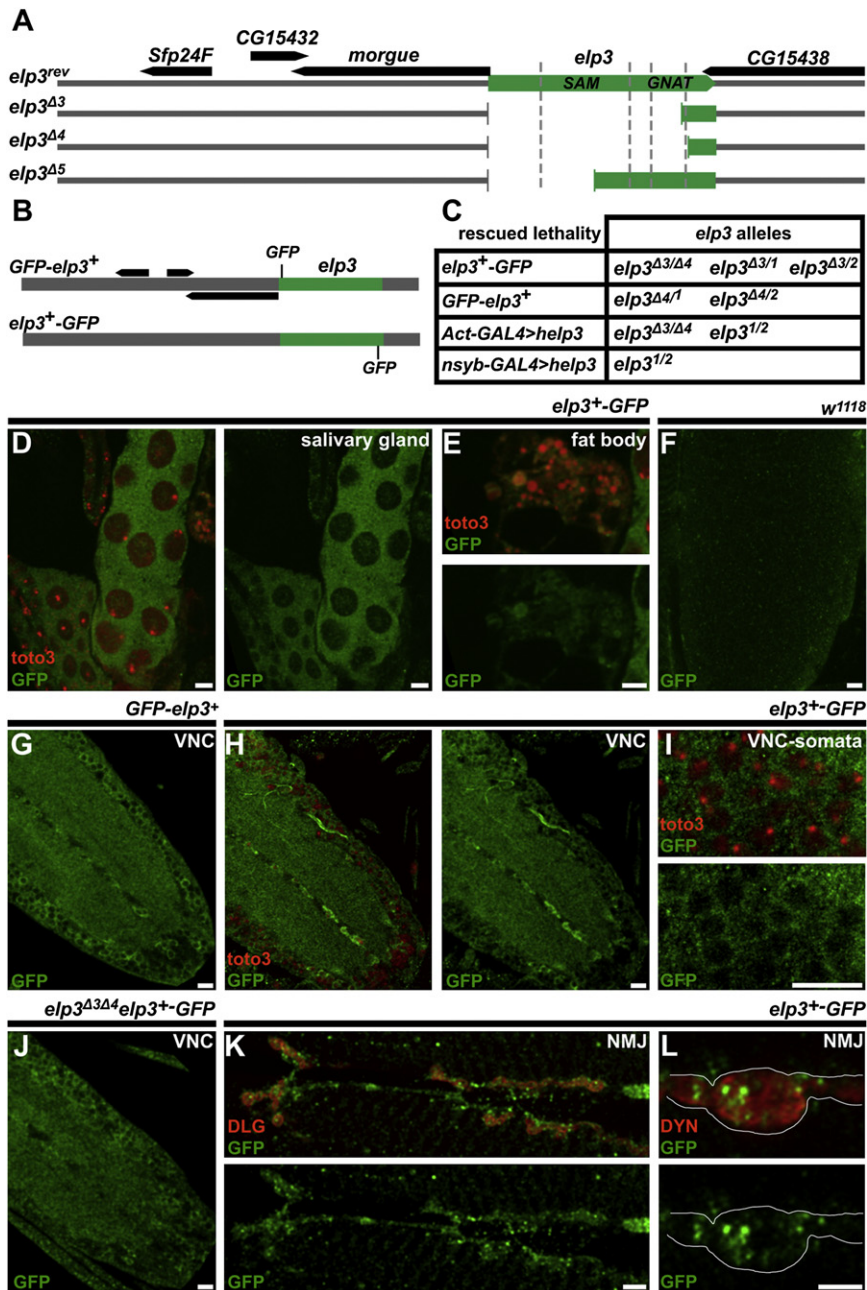
Synapses are highly specialized structures with tightly apposed pre- and postsynaptic elements (Haucke et al., 2011). While the basic building blocks of synapses within a cell may be similar, synaptic contacts are not invariant, and synaptic efficacy of individual release sites differs (Marrus et al., 2004; Peled and Isacoff, 2011; Pelkey et al., 2006; Schmid et al., 2008). This heterogeneity suggests that presynaptic release site function may be locally regulated (Nicoll and Schmitz, 2005; Pelkey and McBain, 2007). Thus, characterization of mechanisms that control the function of individual active zones will yield insight into the regulation of synaptic plasticity in health and disease.

Synaptic vesicles fuse at active zones, specialized presynaptic structures directly aligned to the postsynaptic receptor field (Petersen et al., 1997). In *Drosophila*, active zones harbor electron-dense T bars, and Bruchpilot (BRP), a large cytoskeletal-like protein that is the ortholog of ELKS in mammals, is an integral part of these structures (Hida and Ohtsuka, 2010; Kittel

et al., 2006). BRP self-assembles in macromolecular entities where individual BRP strands join at their N-terminal ends near the plasma membrane while sending their C-terminal ends into the cytoplasm like a parasol (Fouquet et al., 2009; Jiao et al., 2010). Similar to presynaptic specializations in other species, BRP is thought to capture synaptic vesicles using its C-terminal extensions, concentrating synaptic vesicles at active zones and facilitating synaptic transmission (Hallermann et al., 2010b; Zhai and Bellen, 2004). Although the abundance of BRP at individual active zones correlates with the release efficiency (Graf et al., 2009; Marrus et al., 2004; Schmid et al., 2008), little is known about the molecular mechanisms that regulate the function of presynaptic release sites. Here, we identify Elongator protein 3 (ELP3), a member of the elongator complex as a regulator of T bar function and morphology.

ELP3 was originally identified in yeast as a member of the nuclear elongator complex (Otero et al., 1999). ELP3 harbors a Gcn5-related acetyltransferase (GNAT) domain and acetylates lysines in histone H3 (Han et al., 2008; Winkler et al., 2002) to modify DNA chromatin structure (Walia et al., 1998). The ELP3 ortholog in plants is largely nuclear, however, in yeast and several other species, the protein also localizes to the cytoplasm where it is thought to take part in tRNA modification and acetylation of tubulin; however, the mechanistic details are elusive (Creppe et al., 2009; Solinger et al., 2010; Versées et al., 2010). Interestingly, ELP3 polymorphisms have been associated with decreased risk for amyotrophic lateral sclerosis (Simpson et al., 2009), and mutations in ELP1 cause familial dysautonomia (Cheishvili et al., 2011; Slaugenhaupt and Gusella, 2002).

To understand ELP3 function, we have investigated the neuronal role for ELP3 in vitro and in vivo. We show that presynaptic ELP3 loss of function results in altered morphology and function of T bars at fruit fly neuromuscular junctions (NMJs), and this occurs in the absence of defects in tubulin acetylation. We find that T bars in *elp3* mutants change their structure in favor of forming more elaborate cytoplasmic extensions, that more synaptic vesicles are tethered to these T bars, and that neurotransmitter release becomes more efficient, including a larger readily releasable vesicle pool (RRP). Our data indicate that

**Figure 1. ELP3 Localizes to Synapses**

(A and B) *elp3* locus, *elp3* alleles (green) (A), and genomic *elp3* constructs that express GFP N- and C-tagged ELP3 (B). *elp3*^{Δ3} and *elp3*^{Δ4} deletion mutants lack the SAM and GNAT domains, and *elp3*^{Δ5} removes the start codon.

(C) Rescue of lethality of different *elp3* mutants using one copy of GFP-*elp3*⁺ or *elp3*⁺-GFP or using neuronal (*nSyb-GAL4*) or ubiquitous (*Act-GAL4*) expression of *help3*. Lethality scored on regular food while assessing if adult males and females emerged. Expression of *help3* using *BG57-GAL4* (muscular expression) did not rescue lethality (not shown).

(D and E) ELP3 localization using *elp3*⁺-GFP in third-instar larval salivary gland cells and in fat body cells labeled with anti-GFP. DNA is labeled using TOTO3. Scale bars, 10 μm.

(F–J) L3 VNCs of *w*¹¹¹⁸ (F, not GFP-expressing controls), GFP-*elp3*⁺/+ (G), *elp3*⁺-GFP/+ (H and I), and *elp3*^{Δ3/Δ4}, *elp3*⁺-GFP/+ (J) animals labeled with anti-GFP and/or TOTO3. Scale bars, 10 μm (F–H and J) and 5 μm (I).

(K and L) NMJs of *elp3*⁺-GFP/+ animals labeled with anti-GFP and anti-DLG, a pre- and post-synaptic marker (K) or anti-DYN, a presynaptic marker (L). Scale bars, 10 μm (K) and 2.5 μm (L).

by mobilizing *P{SUP or-P}elp3*^{KG02386}, a *P* element inserted in the 5'UTR of *elp3*. We isolated three different deletions of the *elp3* locus (*elp3*^{Δ3}, *elp3*^{Δ4}, *elp3*^{Δ5}) as well as a precise excision (*elp3*^{rev}) that serves as a genetic control (Figure 1A). These deletions fail to complement one another, as well as *elp3*¹ and *elp3*², but not lethal alleles of *morgue*, located 5' of *elp3*. Similar to *elp3* null mutants (*elp3*^{Δ3}/*elp3*^{Δ4}), heteroallelic combinations of the EMS alleles and the *P* element excision alleles die as early pupae, suggesting that all *elp3* alleles we isolated are severe hypomorphic or null alleles (Walker et al., 2011).

To determine if the lethality and phenotypes of the *elp3* alleles are solely due to loss of ELP3 function, we created transgenic flies that harbor genomic *elp3* rescue constructs (Figure 1B) (Venken et al., 2006). The constructs allow expression of a C- or N-terminally GFP-tagged ELP3 under native control (Venken et al., 2008). The presence of *elp3*⁺-GFP or GFP-*elp3*⁺ in several heteroallelic combinations restores viability (Figure 1C; data not shown) and the cellular phenotypes in *elp3* mutants (see below), indicating that only ELP3 function is affected in the mutants tested.

ELP3 is necessary and sufficient for BRP acetylation in vitro and in vivo, and we propose a model where, similar to acetylation of histones, acetylation of BRP regulates the cytoplasmic extensions of T bars, thereby controlling the capture of synaptic vesicles at active zones and neurotransmitter release efficiency.

RESULTS

Elp3 Is an Essential Gene

We previously isolated two EMS alleles of *elp3* (*elp3*¹ and *elp3*²) that harbor missense mutations in the acetyltransferase domain (Simpson et al., 2009) and now created independent null alleles

ELP3 Localizes to the Cytoplasm in Neurons and Enriches at Synapses

To determine the subcellular localization of *Drosophila* ELP3, we labeled *elp3*⁺-GFP and GFP-*elp3*⁺ with several markers and

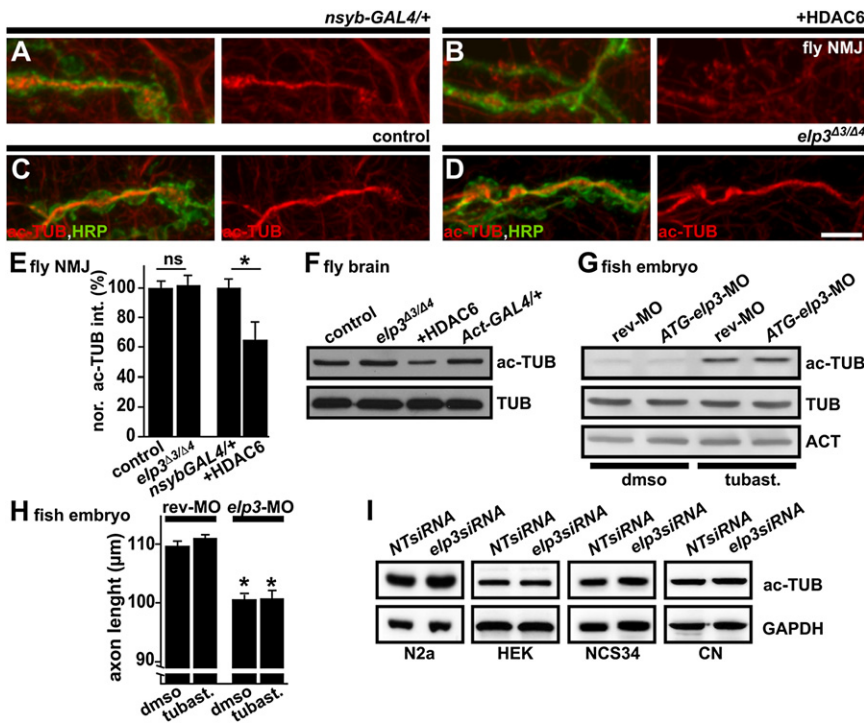


Figure 2. Tubulin Acetylation Is Not Affected upon Loss of ELP3 Function

(A–E) NMJs of *y w; nSyb-GAL4/+* (A), *y w; UAS-hdac6/+; nSyb-GAL4/+* (B), control *y w; elp3^{rev}* (C), and mutant *y w; elp3^{Δ3/Δ4}* (D) *Drosophila* L3 larvae labeled with anti-acetylated tubulin (ac-TUB) (red) and anti-HRP (green), a neuronal membrane marker; and (E) quantification of acetylated tubulin intensity in bouton: mean ac-TUB intensity relative to anti-HRP intensity normalized to control (%). Mean is quantified from six to ten NMJs from at least four animals. Error bars, SEM. t test, **p* < 0.05. Scale bar, 5 μm. ns, not significant. Related to Figure S1.

(F) Western blot of brains dissected from control, *y w; elp3^{rev}*, *y w; elp3^{Δ3/Δ4}*, *y w; Act-GAL4/+; y w; UAS-hdac6/+; Act-GAL4/+* (+HDAC6) *Drosophila* third-instar larvae labeled with antibodies against ac-TUB and total tubulin (TUB).

(G) Western blot of zebrafish 30 hpf embryos injected with *elp3* (*elp3*-MO) and control (rev-MO) morpholinos, and either incubated in DMSO (control) or in tubastatin A (tubast.). Blots were probed with anti ac-TUB, TUB, or Actin (ACT).

(H) Quantification of axonal length of 30 hpf zebrafish embryos after injection of control (rev-MO) or *elp3* (*elp3*-MO) morpholinos, treated with DMSO (control) or tubastatin A (tubast.). t test, **p* < 0.05.

(I) Western blot of N2a, HEK, NCS34, and cultured cortical neuron cells (CN) transfected with *elp3*siRNA or nontargeting NT-siRNA (controls), probed with ac-TUB and GAPDH (control) antibodies. Related to Figure S1.

assessed GFP distribution. While control animals not expressing GFP do not show labeling (Figure 1F; data not shown), in several cell types of third-instar larvae, including salivary gland cells and fat body cells, ELP3-GFP as well as GFP-ELP3 label the nucleus and/or the cytoplasm (Figures 1D and 1E; data not shown). In contrast, in neurons of the ventral nerve cord (VNC) in third-instar larvae, we observe abundant ELP3 that concentrates in the cytoplasm, and we do not observe much nuclear labeling overlapping with Toto-3, a DNA marker. Furthermore, our data indicate that ELP3 concentrates in the synaptic-rich areas of the VNC and overlaps with the synaptic markers anti-Discs Large (DLG) and anti-Dynamin (DYN; Figures 1G–1J; data not shown). Similarly, also in mouse motor neurons in culture, we observe abundant cytoplasmic ELP3 localization, indicating that this feature is evolutionary conserved (data not shown). In *Drosophila* larvae, ELP3-GFP is also present at the presynaptic side of NMJ boutons, double labeled with anti-DLG or with anti-DYN (Figures 1K and 1L). Thus, our data suggest a cytoplasmic role for ELP3 in motor neurons.

To test whether ELP3 plays an important role in the nervous system, we generated transgenic animals that harbor a UAS-human ELP3 construct. Driving expression of hELP3 ubiquitously using *Act-Gal4* rescues lethality associated with *elp3* loss of function (*elp3¹/elp3²*; *elp3^{Δ3}/elp3^{Δ4}*), and these flies show normal electroretinogram recordings (data not shown) (Simpson et al., 2009), indicating that the construct is functional (Figure 1C). Driving hELP3 specifically in the nervous system using *nsyb-Gal4* also rescues lethality of *elp3* heteroallelic

combinations (Figure 1C, and see also below). In contrast, muscular hELP3 expression using *BG57-Gal4* does not restore viability (data not shown). These data indicate an important role for ELP3 in the nervous system and presynaptically at the NMJ and also suggest that the function of ELP3 is evolutionary conserved.

Tubulin Acetylation Is Normal in *elp3* Null Mutant Larvae

ELP3 harbors an acetyltransferase domain, and recent evidence suggests that this function is important to mediate tubulin acetylation (Creppe et al., 2009; Solinger et al., 2010). To test if ELP3 plays a role in neuronal tubulin acetylation in vivo, we labeled acetylated tubulin with specific antibodies in controls and *elp3* null mutant *Drosophila* larvae. As a control we overexpressed HDAC6 (*nsyb-GAL4*), previously shown to act as a tubulin deacetylase (Hubbert et al., 2002). While neuronal HDAC6 overexpression results in reduced acetylated tubulin labeling in motor neurons (Figures 2A, 2B, and 2E), loss of ELP3 function does not result in a difference in labeling intensity (Figures 2C–2E; see Figures S1A–S1C available online). Similarly, western blot of acetylated tubulin also does not show a difference between *elp3* null mutants and controls (Figure 2F). Furthermore, kinesin-driven axonal transport of synaptic vesicles, thought to be regulated by microtubule acetylation, is also not affected in *elp3* mutants (Figures S1D–S1F), indicating that acetylation of microtubules in *Drosophila* larvae that lack *elp3* is not affected.

To test if ELP3 is involved in tubulin acetylation in vertebrates, we performed western blots using extracts of zebrafish embryos

(30 hr post-fertilization [hpf]) treated with *elp3* morpholinos or treated with control morpholinos (Figure 2G). As we reported before, *elp3* morpholino treatment results in reduced motor axon length at 30 hpf (Simpson et al., 2009) (Figure 2H). However, *elp3* knockdown does not show reduced levels of acetylated tubulin (Figure 2G). Consistently, treatment of fish with tubastatin, a specific inhibitor of HDAC6-mediated tubulin deacetylation, results in the expected increase in acetylated tubulin levels, but *elp3* morpholino treatment does not counteract this effect (Figure 2G). Furthermore, tubastatin treatment fails to rescue *elp3* morpholino-induced reduction in motor neuron axon length (Figure 2H), indicating that motor axon extension phenotypes upon *elp3* morpholino treatment are not caused by decreased tubulin acetylation. Finally, we also assessed a role for ELP3 in the acetylation of microtubules in N2a, HEK, and NCS34 neuroblastoma cells as well as in mouse cortical neurons or motor neurons using *elp3*-siRNA or *elp3*-shRNA but did not observe a decrease in the acetylation status of microtubules (Figure 2I; Figures S1G–S1P). Thus, using different species and cell types, our data indicate that ELP3 is not a major acetyltransferase for tubulin, and suggest that ELP3 exerts neuronal functions without affecting tubulin acetylation.

BRP Spots Are Enlarged at *elp3* Mutant NMJs

Given the cytoplasmic and synaptic localization of ELP3 in neurons, we assessed the abundance and localization of various markers at the *Drosophila* third-instar larval NMJ. We labeled control and *elp3* mutant synapses with the periaxonal zone marker anti-FasciclinII (FASII), the synaptic vesicle markers anti-Cysteine string protein (CSP), anti-synaptobrevin (nSYB), and anti-vesicular glutamate transporter (vGLUT), with the endocytic marker anti-DYN and with the active zone markers anti-BRP^{NC82}, anti-Liprin- α (LIP), and Cacophony-GFP (CAC). While most of the markers tested do not display a quantitative difference in labeling intensity or localization in *elp3* mutants compared to controls, BRP^{NC82} immunoreactivity is markedly increased (Figures 3A–3D, 3G; Figures S2A–S2D), and this defect is specific to loss of *elp3*, as adding a wild-type copy of *elp3* completely rescues the defect (Figures 3D, 3E, and 3G; data not shown). BRP^{NC82} recognizes BRP, an integral member of the electron-dense T bar within the active zone where synaptic vesicles fuse with the membrane (Figure 3H). However, given that other active zone markers including LIP and CAC do not show differences in labeling (Figures 3B, 3C, and 3G), our data indicate specific synaptic defects in *elp3* mutants, including increased BRP^{NC82} immunoreactivity at NMJ boutons.

BRP forms macromolecular assemblies that are involved in shaping the T bar (Fouquet et al., 2009). Several “BRP strands” join at their N-terminal ends and contact Cacophony calcium channels near the presynaptic membrane (Kittel et al., 2006), while BRP C-terminal ends extend into the cytoplasm (Figure 3H). BRP^{NC82} antibodies label the BRP C-terminal portion, while anti-BRP^N antibodies label the N-terminal end of the protein (Fouquet et al., 2009). To further quantify the defect in BRP^{NC82} labeling, we measured dot number in controls and *elp3* mutants. As shown in Figure 3J, we do not observe an increase in the number of BRP^{NC82} dots per bouton area in

elp3 mutants, and similarly, we also do not find a difference in the densities of dots per bouton of other active zone markers including LIP and CAC in *elp3* mutants and controls (Figures 3B, 3C, 3L, and 3M), indicating that *elp3* mutations do not affect the number of active zones per synaptic area. Furthermore, compared to controls, we also do not observe altered calcium influx measured using GCaMP3 (Tian et al., 2009) in *elp3* mutant boutons (Figures S2E–S2G), in line with normal calcium channel clustering and function in the mutants.

Next, we quantified BRP^{NC82} dot size (maximum diameter) in controls and *elp3* null mutants and found an overall increase in the size of individual BRP^{NC82} dots (Figures 3D and 3N), suggesting increased immunoreactivity of this antigen at individual active zones. To scrutinize the BRP defect in *elp3* mutants in more detail, we also quantified features of BRP^N labeling in controls and *elp3* mutants (Figures 3F, 3H, 3K, and 3O). First, we quantified the number of BRP^N dots per bouton area but did not find a difference, again indicating that ELP3 does not affect the number of active zones per bouton area (Figure 3K). Next, we also quantified BRP^N dot size, but in contrast to BRP^{NC82} labeling, BRP dot size revealed by BRP^N is very similar at *elp3* mutant boutons and controls (Figure 3O), suggesting that T bar assembly per se (the number of BRP molecules) is not affected in *elp3* mutants. We further assessed if in *elp3* mutants supernumerous “BRP strands” join (Figure 3H), by also performing western blots of *elp3* mutant and control brains probed with different BRP antibodies but found very similar BRP levels (Figure 3I; data not shown). Thus, the data indicate normal assembly of BRP strands at active zones and are consistent with morphological alterations at the C-terminal of BRP resulting in a more accessible BRP^{NC82} epitope in *elp3* mutants.

Active Zones Are Malformed in *elp3* Mutants

To directly assess active zone morphology in *elp3* mutant and controls, we performed transmission electron microscopy (TEM). Quantification of several synaptic features, including synaptic vesicle number, synaptic vesicle size, mitochondrial number, and T bar number, does not reveal major differences between mutants and controls (Figures 4A–4C; Figure S3), indicating that *elp3* mutations do not result in widespread synaptic defects or affect synaptic organelle transport. The most prominent feature in *elp3* mutant boutons is the occurrence of sizable T bars with large protrusions that extend into the cytoplasm (Figures 4D–4G, arrows). Quantification of T bar top lengths (platforms) in controls indicates that they never exceed 300 nm, while in *elp3* mutants we observe more than 20% of the T bars with a platform that is larger than 300 nm and up to 400 nm in length (Figures 4D–4G, arrowheads; Figure 4H). Thus, TEM indicates an increase in T bar size in *elp3* mutants, and these data are consistent with the extensive “tentacles” extending into the cytoplasm in *elp3* mutants that we observe in electron tomograms of *elp3* mutant boutons (Figures 4I–4O, arrows). In line with these data, we measure a concomitant increase in the number of synaptic vesicles that are in direct contact with the T bar (Figure 4P). Hence, the elaboration of the dense projections of the T bar in *elp3* mutants results in an increased number of T bar-tethered vesicles.

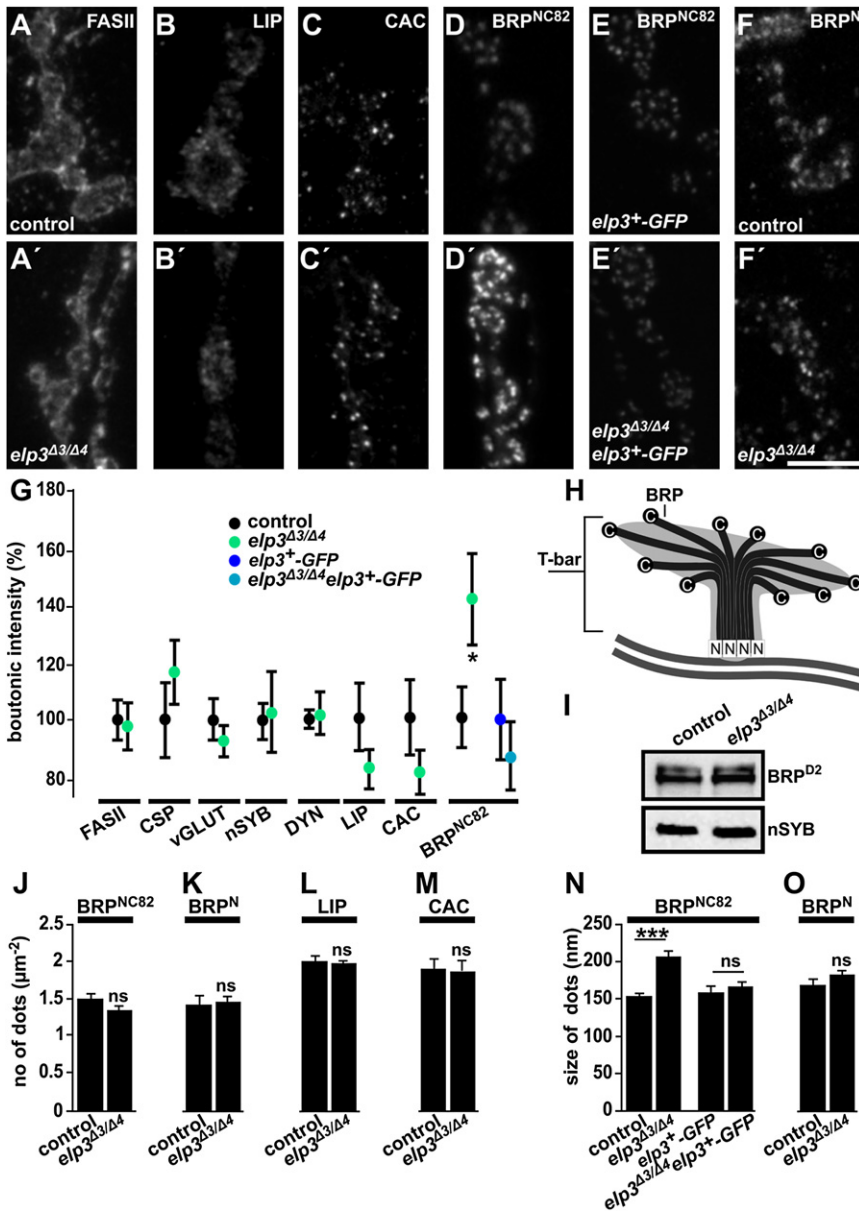


Figure 3. Bruchpilot BRP^{NC82} Immunoreactivity Is Expanded in *elp3* Mutants, while Other Synaptic Markers Are Not Affected

(A–F) Labeling of *Drosophila* third-instar NMJs of *y w; elp3*^{rev} (control A–D and F) and *y w; elp3*^{Δ3/Δ4} (A'–D' and F') with anti-HRP (neuronal membranes) or anti-DLG (not shown), and FasciclinII, a perisynaptic marker (FASII) or the active zones proteins: Liprin-α (LIP), Cacophony-GFP (CAC), and Bruchpilot (BRP^{NC82} and BRP^N); and of *y w; elp3*^{rev/+}; *elp3*^{Δ3/Δ4}*elp3*^{Δ3/Δ4} (*elp3*^{Δ3/Δ4}*elp3*^{Δ3/Δ4}, control) and *y w; elp3*^{Δ3/Δ4}; *elp3*^{Δ3/Δ4}*elp3*^{Δ3/Δ4} rescued animals with BRP^{NC82} (E and E'). Related to Figure S2. Scale bar, 5 μm (A–F, in F').

(G) Quantification of synaptic marker intensity (genotypes in A–E), relative to anti-HRP intensity (not shown) and of synaptic vesicle markers Cysteine string protein (CSP), Vesicular glutamate transporter (vGLUT), and Synaptobrevin (nSYB) and Dynamin (DYN) (Figures S2A–S2D). Data are normalized to control (%). Mean is quantified from six to ten NMJs from at least four animals. Error bars, SEM. t test, *p < 0.05.

(H) Schematic of a T bar indicating the BRP-N and -C terminals. Double line shows presynaptic membrane.

(I) Western blot of brains dissected from control, *y w; elp3*^{rev} and *y w; elp3*^{Δ3/Δ4} L3 larvae labeled with BRP^{D2} and nSYB (control).

(J–M) Quantification of the dot number per synaptic area (defined by anti-HRP or anti-DLG) for BRP^{NC82} (J), BRP^N (K), LIP (L), and CAC-GFP detected with anti-GFP (CAC, M). Mean is quantified from five to ten NMJs from at least four animals. Error bars, SEM. t test, p > 0.05. ns, not significant.

(N and O) Quantification of BRP^{NC82} dot size in controls, *y w; elp3*^{rev} and mutants, *y w; elp3*^{Δ3/Δ4} as well as in controls, *y w; elp3*^{rev/+}; *elp3*^{Δ3/Δ4}*elp3*^{Δ3/Δ4} (*elp3*^{Δ3/Δ4}*elp3*^{Δ3/Δ4}) and rescued animals, *y w; elp3*^{Δ3/Δ4}; *elp3*^{Δ3/Δ4}*elp3*^{Δ3/Δ4} (N); and quantification of BRP^N dot size in controls and *y w; elp3*^{Δ3/Δ4} mutants (O). Mean is quantified for five to ten NMJs from at least four animals. Error bars, SEM. t test, ***p < 0.0001. ns, not significant.

Loss of *elp3* Results in Larger Excitatory Junctional Currents and Miniature Excitatory Junctional Currents

To determine functional consequences associated with the loss of *elp3* at the NMJ, we measured synaptic transmission using two electrode voltage clamp. The average excitatory junctional current (EJC) amplitude in 0.45 mM calcium is significantly increased in *elp3* mutants (Figures 5A and 5B), and also current clamp recordings indicate increased excitatory junctional potential amplitudes in *elp3* mutants compared to controls (Figure S4).

To determine quantal content, we measured spontaneous vesicle fusion (mEJC) and quantified the quantal amplitude. As shown in Figures 5C–5F, mEJC amplitudes are significantly increased in *elp3* mutants compared to controls, while the mEJC frequency trends toward an increase, but this is not statis-

tically significant. The quantal content (in 0.45 mM calcium) also trends toward an increase but is not significantly different in controls and mutants (EJC/mEJC; controls, 45.3 ± 3.5 quanta; *elp3*^{Δ3/Δ4}, 54.6 ± 6.7 quanta). Increased mEJC amplitude can be caused by larger synaptic vesicles that harbor more neurotransmitter or by a more elaborate postsynaptic glutamate receptor field. Given that synaptic vesicle size distribution in *elp3* mutant NMJs is not different from controls, we labeled *elp3* mutant NMJs with anti-GluRIIA^{8B4D2} antibodies and with anti-GluRIII/IIC antibodies that each recognize different glutamate receptor subunits (DiAntonio et al., 1999; Marrus et al., 2004). While we did not observe a difference in GluRIII/IIC labeling between *elp3* mutants and controls (Figures 5G, 5H, and 5M), the GluRIIA labeling in *elp3* mutants is increased compared

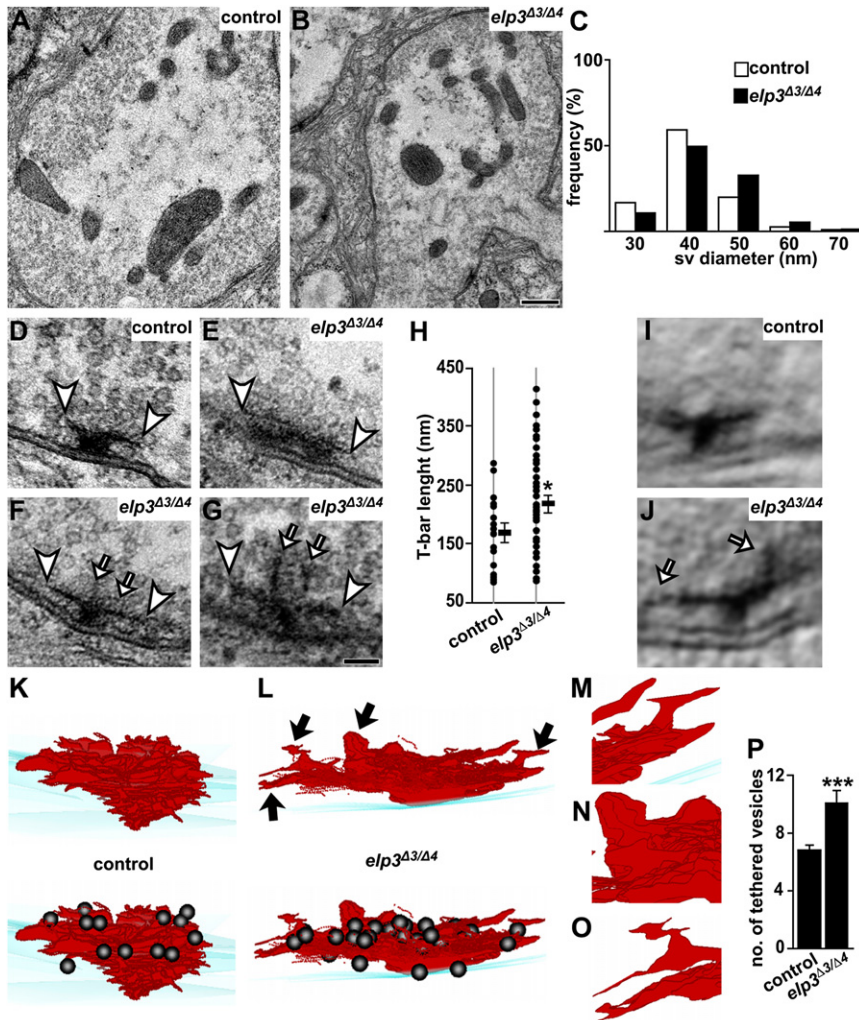


Figure 4. T Bars Send Extensive Tentacles into the Cytoplasm in *elp3* Mutants

(A–H) TEM of NMJ boutons of *y w; elp3^{ev}* control (A and D) and *y w; elp3^{Δ3/Δ4}* mutants (B and E–G). Synaptic vesicle diameter frequency (C) from >2134 vesicles from >20 boutons from 3 animals per genotype. (D–G) High-magnification image of T bars in controls (D) and *elp3^{Δ3/Δ4}* mutants (E–G) and distribution of individual T bar top lengths (arrowheads in D–G) and their averages \pm SEM (H). Mean is quantified for >17 T bars from 3 animals per genotype. t test, * $p < 0.05$. Related to Figure S3. Scale bars, 0.5 μ m (A and B) and 0.1 μ m (D–G).

(I and J) Electron tomogram of a T bar from *y w; elp3^{ev}* (I) and from *y w; elp3^{Δ3/Δ4}* mutant (J). A total of 40 Z slices are projected. Arrows indicate tentacles extending in the cytoplasm in *elp3* mutants.

(K–O) 3D reconstructions of T bars shown in (I) and (J) in *y w; elp3^{ev}* (K) and in *y w; elp3^{Δ3/Δ4}* mutants (L–O). Arrows indicate cytoplasmic extensions, magnified in (M)–(O). T bars are shown frontally (looking from the cytoplasm to the presynaptic membrane [light blue]) in their longest dimension, turned by 30° along the y axis showing the side and top.

(P) Quantification of the number of T bar-tethered synaptic vesicles. Mean is quantified for >17 T bars from 3 animals per genotype. Error bars, SEM. t test, *** $p < 0.0001$.

to controls, and this defect is rescued by a genomic fragment that harbors wild-type *elp3* (Figures 5I–5M). These data are consistent with the increased mEJC amplitude in *elp3* mutants to be caused by exuberant GluRIIA clustering.

Presynaptic Loss of *elp3* Results in a Larger RRP

The number of T bar-tethered synaptic vesicles in *elp3* is increased, and we tested whether a larger pool of synaptic vesicles is immediately ready for fusion in the mutants. First, we used fluctuation analysis to estimate the number of release-ready vesicles in controls and *elp3* mutants. Given that EJC amplitudes in *elp3* mutants and controls saturate at high calcium (Figure S5A), we performed this analysis in the presence of a rapidly dissociating competitive receptor antagonist γ -D-glutamylglycine (γ -DGG) that has been used at the *Drosophila* larval NMJ before (Pawlu et al., 2004). As shown in Figure S5A, EJC amplitudes recorded in 5 mM external calcium are reduced by 38% when incubated in 10 mM γ DGG, and also mEJC amplitudes (recorded in 0.5 mM Ca^{2+}) are smaller both in controls (without γ DGG 1.08 \pm 0.05 nA; with γ DGG 0.68 \pm 0.05 nA; Figure S5B) as well as in *elp3* mutants (without γ DGG 1.29 \pm 0.07 nA; with

least in part prevents postsynaptic receptor saturation in high calcium concentrations. Recordings in the presence of the drug will thus allow us to assess neurotransmitter release while partly suppressing glutamate receptor saturation in controls and mutants.

We then recorded EJC amplitudes in γ DGG and different calcium concentrations and extracted quantal parameters from parabolic fits from EJC variance versus EJC mean amplitude plots (Figures S5C and S5D) (Foster and Regehr, 2004). Our data indicate a larger release-ready pool in *elp3* mutants compared to controls (controls, 512.7 \pm 35.1 quanta; *elp3*, 592.2 \pm 41.3 quanta; $p < 0.05$). Also, we find a similar release probability (Pr) in controls and mutants in low calcium concentrations (Ca^{2+}): (0.3 mM) control 0.08 \pm 0.001 and *elp3* 0.13 \pm 0.01; (0.4 mM) control 0.20 \pm 0.01 and *elp3* 0.17 \pm 0.01; and (0.6 mM) control 0.27 \pm 0.02 and *elp3* 0.24 \pm 0.03. Similarly, in 3 mM calcium our analyses indicate a similar Pr (control, 0.98 \pm 0.02; *elp3*, 0.96 \pm 0.02), but under these conditions, postsynaptic receptor desaturation by γ DGG may be incomplete (Figure S5A), confounding our estimations of the release-ready pool and Pr in the mutants. Nonetheless, in high calcium, Pr is invariably high,

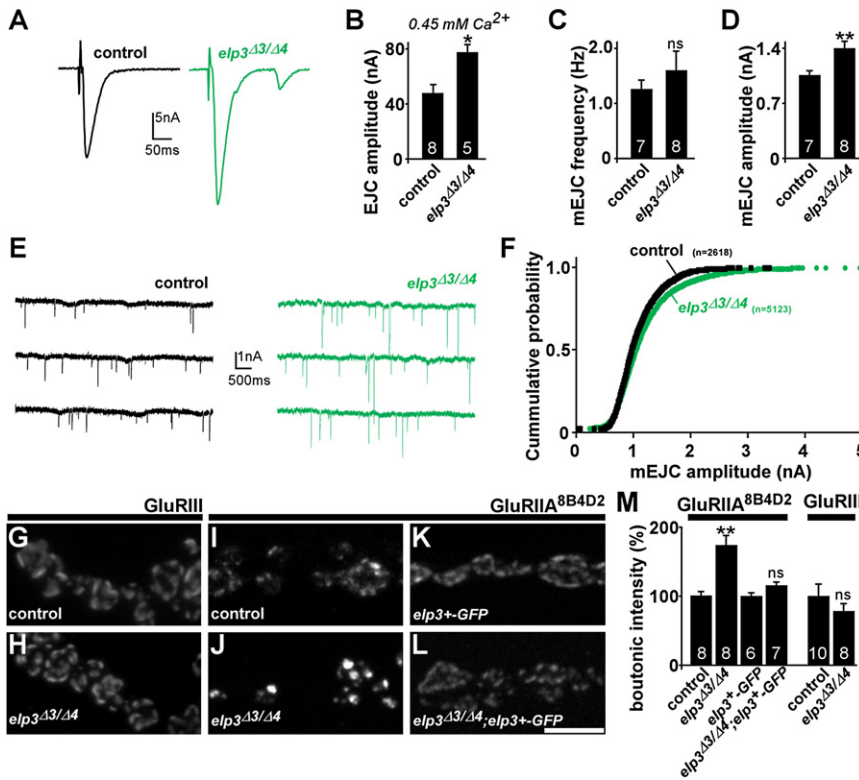


Figure 5. EJC and mEJC Amplitude Are Increased in *elp3* Mutants

(A and B) Sample EJCs (A) from control *y w; elp3^{rev}* and mutant *y w; elp3^{Δ3/Δ4}* animals recorded in 0.45 mM CaCl₂ and quantification of the mean EJC amplitude (B). Error bars, SEM. n, number of animals tested. t test, *p < 0.05. Related to Figure S4.

(C–F) mEJCs recorded in 0.5 mM CaCl₂ with TTX in control *y w; elp3^{rev}* (black) and mutant *y w; elp3^{Δ3/Δ4}* (green) animals; quantification of the mean mEJC frequency (C) and amplitude (D), sample EJC traces (E), and cumulative probability histograms of mEJC amplitude (F; the number of mEJCs included is indicated). Error bars, SEM. n, number of animals tested. t test, **p < 0.01; ns, not significant.

(G–L) Labeling of *y w; elp3^{rev}* (control, G and I), *y w; elp3^{Δ3/Δ4}* (H and J), *y w; elp3^{rev/+}; elp3⁺-GFP/+* (*elp3⁺-GFP*), K), and *y w; elp3^{Δ3/Δ4}; elp3⁺-GFP/+* (rescued *elp3* mutants, L) *Drosophila* NMJs with anti-GluRIII (G and H), anti-GluRIIA^{8B4D2} (I–L), and anti-HRP or anti-DLG (not shown). Scale bar, 5 μm for (G)–(L) in (L).

(M) Quantification of GluR intensity relative to anti-HRP or anti-DLG intensity. Data are normalized to control (%), and mean is quantified from six to ten NMJs from more than four animals. Error bars, SEM. Student's t test, **p < 0.01. ns, not significant.

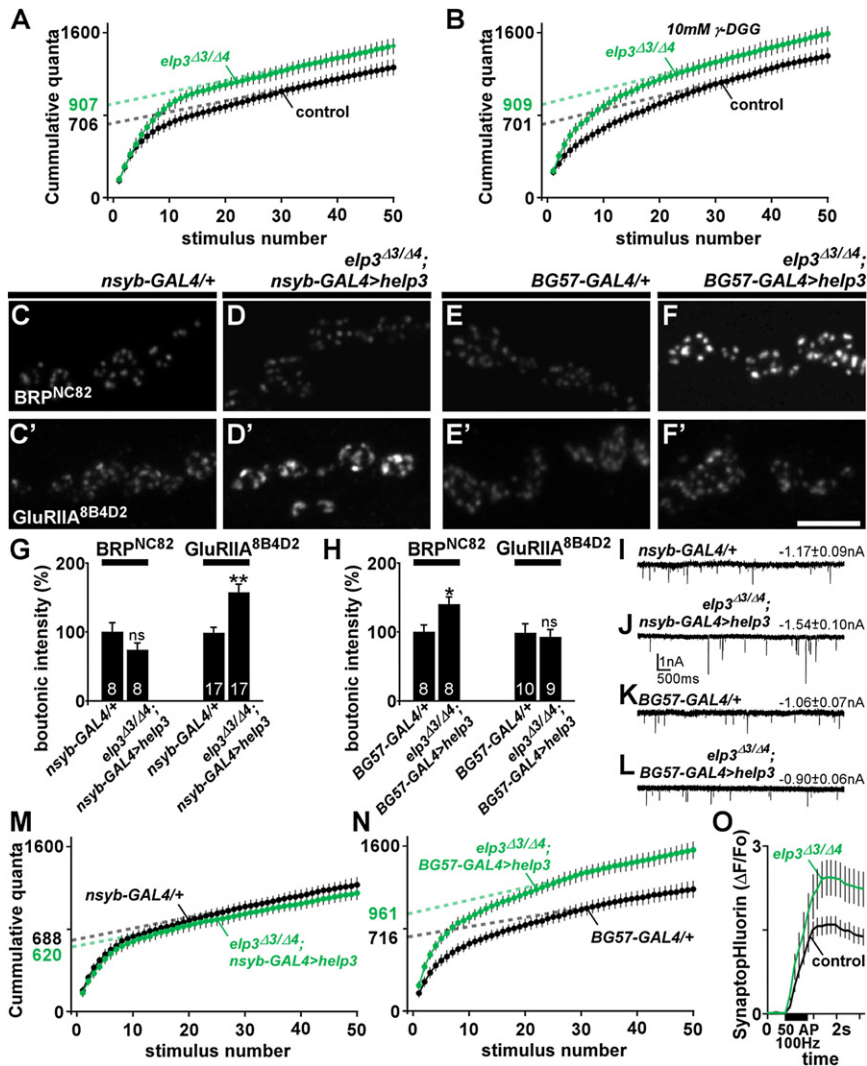
and differences in Pr, if any, between *elp3* mutants and controls remain small.

To independently evaluate presynaptic release properties, we also measured transmission during a short train of high-frequency stimulation (500 ms, 100 Hz) in 5 mM external calcium, ensuring a high Pr (Figure 6A). This protocol results in the release of neurotransmitters from vesicles that are ready for fusion during the first stimulations and, subsequently, reveals the rate at which new vesicles are captured and prepared for release (30th–50th stimulation) (Haller mann et al., 2010a). While the rate at which vesicles are refilled into the releasable pool during this stimulation paradigm is similar in *elp3* mutants and controls (p > 0.05), back extrapolation from linear fits of the cumulative quantal content between the 30th and 50th stimulation reveals a larger pool of quanta that readily fuses in *elp3* mutants compared to controls (control, 706.1 ± 36.9 quanta; *elp3*, 907.5 ± 52.2 quanta; p < 0.05). This effect is likely not caused by a postsynaptic change in receptor sensitivity as mEJC amplitude distribution in controls and in *elp3* mutants before versus immediately following stimulation is similar (Figures S5E and S5F). Finally, we also recorded EJCs during a 500 ms 100 Hz train in the presence of γDGG, allowing us to perform recordings where the Pr is high, but postsynaptic receptor saturating is partly inhibited (Figures S5A–S5C). As shown in Figure 6B, recordings in γDGG yield very similar results for the sizes of the RRP compared to recordings in the absence of the drug (control, 700.8 ± 27.5 quanta; *elp3*, 909.1 ± 40.7 quanta; p < 0.05). While γDGG may not completely block receptor saturation in high calcium, the data suggest that changes in postsynaptic receptor

saturation are not the major cause of the larger number of detected quanta in *elp3* mutants.

To determine the relative contribution of pre- or postsynaptic loss of *elp3* to the defect we observe during high-frequency stimulation, we conducted rescue experiments. We expressed wild-type ELP3 (hELP3) using *nsyb-Gal4* only in neurons (presynaptically at the NMJ) or using *BG57-Gal4* only in muscles (postsynaptically at the NMJ) in *elp3* null mutants. While neuronal expression of ELP3 rescues the increased BRP^{NC82} immunoreactivity (Figures 6C, 6D, and 6G), but not the GluRIIA^{8B4D2} defect (Figures 6C', 6D', and 6G), muscular expression fails to rescue the BRP^{NC82} defect (Figures 6E, 6F, and 6H) but rescues the GluRIIA^{8B4D2} defect (Figures 6E', 6F', and 6H). Furthermore, muscular expression of ELP3 rescues the increased mEJCs seen in *elp3* mutants, but neuronal ELP3 expression does not (Figures 6I–6L). Thus, ELP3 is cell autonomously required in neurons to regulate BRP morphology and in muscles to restrict GluRIIA abundance.

Having established conditions where the postsynaptic GluRIIA defect is rescued and the presynaptic defect at the level of BRP is not, we evaluated the number of readily released quanta during a 500 ms 100 Hz stimulation train by back extrapolation. We find that expression of ELP3 in the nervous system of *elp3* null mutants rescues the increased release seen in *elp3* mutants (*nsyb-Gal4/+*, 688.1 ± 43.3; *elp3 nsyb-Gal4*, 620.2 ± 32.6; p > 0.05) (Figures 6A and 6M). Conversely, when we assess the number of readily released quanta in *elp3* mutants that express ELP3 in muscles, the pool size is still large (*BG57/+*, 716.3 ± 44.7; *elp3 BG57*, 961.3 ± 18.7; p < 0.05) (Figures 6A



SpH expressed in *elp3* mutants (*y w; elp3^{Δ3/Δ4}; nsyb-GAL4/UAS-SpH*, green) and in controls (*y w; nsyb-GAL4/UAS-SpH*, black) prior to, during, and following a 500 ms 100 Hz stimulation train (black bar). Error bars, SEM; *n* = 9. ANOVA, *p* < 0.01. Related to Figure S5.

and 6N). Thus, the data indicate that the larger pool of quanta released under these conditions in *elp3* mutants stems from a presynaptic defect.

To independently test for a presynaptic defect in vesicle release in *elp3* mutants, we expressed synaptopHluorin (SpH). SpH is a synaptic vesicle-associated pH sensor. At low vesicular pH, SpH GFP is quenched but increases in fluorescence upon vesicle fusion (Miesenböck et al., 1998). We monitored SpH fluorescence during a 500 ms 100 Hz stimulation paradigm, and while the initial baseline fluorescence (F_0) in controls and *elp3* mutants is similar (data not shown), GFP fluorescence increases to a much higher level in *elp3* mutants compared to controls (Figure 6O). The data indicate that significantly more synaptic vesicles in *elp3* mutants fuse during such a bout of stimulation. We do not believe that the increased fluorescence we observe is the result of defects in endocytosis in *elp3* mutants, as our analyses have not revealed endocytic defects in the mutants (data

not shown), and in addition, a potential defect in endocytosis would not be expected to significantly contribute to the increase in fluorescence within this short time period.

ELP3 Is Necessary and Sufficient for BRP Acetylation

Given that *elp3* mutants show morphological defects at the level of their T bars, we tested whether BRP is a substrate for ELP3-dependent acetylation. First, we expressed *Drosophila* HIS-ELP3 in *E. coli*, purified, and refolded the protein (Figures S6A and S6B). Acetyltransferases are prone to autoacetylation (Choudhary et al., 2009). We therefore incubated ELP3 with 20 mM Acetyl-CoA for various time periods. Western blots probed with antibodies against acetylated lysine (Ac-K) indicate time-dependent ELP3 autoacetylation (Figure 7A). Next, we tested whether our ELP3 protein can acetylate purified histone H3, a well-established target, and tubulin. Our data indicate both concentration- and time-dependent acetylation of histone

Figure 6. Presynaptically, the Size of the RRP Is Increased in *elp3* Mutants

(A and B) The cumulative released quanta recorded at 100 Hz in 5 mM $CaCl_2$ without (A) or with γ DGG (B) versus stimulus number in control (*y w; elp3^{ev/+}*, black) and *y w; elp3^{Δ3/Δ4}* mutant (green) animals. The y-intercept of the slope of the trend line (dotted line) at steady state (points 30–50) provides a measure of the average RRP size (indicated, control: black, *elp3*: green). Error bars, SEM; *n* > 7.

(C–H) Images (C–F) and quantification of labeling intensity (G and H) in *y w; elp3^{ev/+}; nsyb-GAL4/+* (control, C and C'), *y w; elp3^{Δ3/Δ4} UAS-help3; nsyb-GAL4/+* (*elp3* mutant with neuronal ELP3 expression; D and D'), *y w; elp3^{ev/+}; BG57-GAL4/+* (control, E and E'), and *y w; elp3^{Δ3/Δ4} UAS-help3; BG57-GAL4/+* (*elp3* mutant with muscular ELP3 expression F and F') with anti-BRP^{NC82} (C–F) or anti-GluRIIA^{8B4D2} (C'–F'). Scale bar, 5 μ m (C)–(F) in (F'). Mean bouton BRP or GluRIIA intensity relative to anti-HRP, and data are normalized to control (%). *n*, number of NMJs from at least four animals (indicated in the bars). Error bars, SEM. \dagger test, $\ast p < 0.05$, $\ast\ast p < 0.001$. ns, not significant.

(I–L) mEJC traces of recordings in 0.5 mM $CaCl_2$ with TTX in *y w; elp3^{ev/+}; nsyb-GAL4/+* (I), *y w; elp3^{Δ3/Δ4} UAS-help3; nsyb-GAL4/+* (J), *y w; elp3^{ev/+}; BG57-GAL4/+* (K), and *y w; elp3^{Δ3/Δ4} UAS-help3; BG57-GAL4/+* (L). Mean mEJC amplitudes \pm SEM; *n* > 6 animals.

(M and N) The cumulative released quanta recorded at 100 Hz in 5 mM $CaCl_2$ in control *y w; elp3^{ev/+}; nsyb-GAL4/+* (M, black), *y w; elp3^{Δ3/Δ4} UAS-help3; nsyb-GAL4/+* (M, green), control *y w; elp3^{ev/+}; BG57-GAL4/+* (N, black), and *y w; elp3^{Δ3/Δ4} UAS-help3; BG57-GAL4/+* (N, green). The y-intercept of the slope of the trend line (dotted lines) at steady state (points 30–50) is a measure of the average RRP size (indicated). Error bars, SEM; *n* > 6 animals.

(O) Mean relative fluorescence change ($\Delta F/F_0$) of

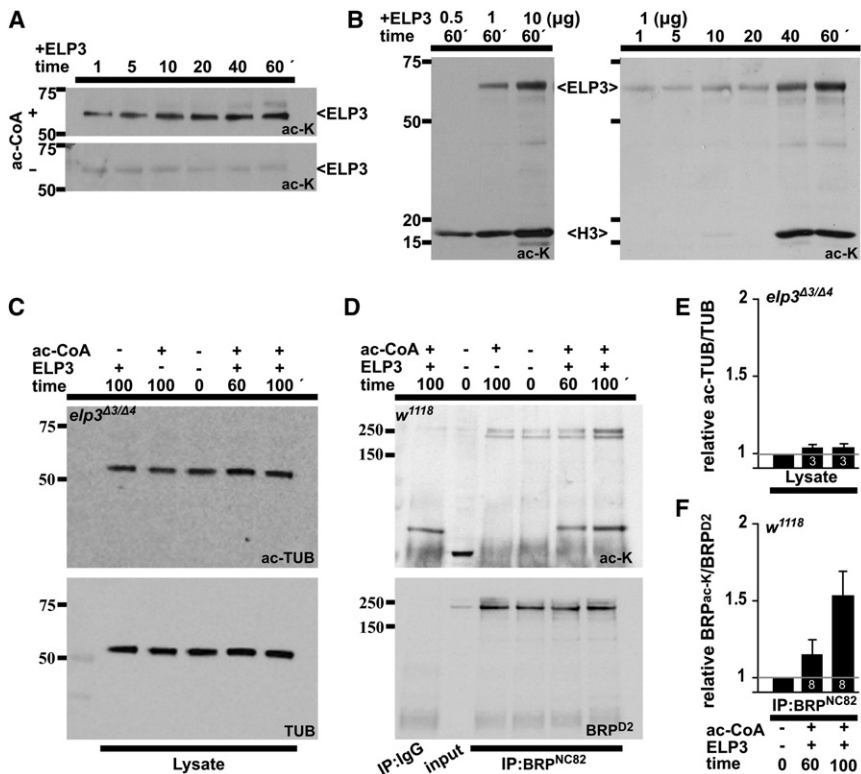


Figure 7. ELP3 Is Sufficient to Acetylate BRP

(A) Autoacetylation of ELP3 using an ELP3-enriched fraction with and without adding Acetyl CoenzymeA (ac-CoA); western blots probed with Ac-K. Related to Figure S6.

(B) Time-dependent and concentration-dependent in vitro acetylation of histone H3 with an ELP3-enriched fraction; western blots were probed with Ac-K.

(C) Tubulin acetylation assay with an ELP3-enriched fraction on brain extracts of third-instar *y w*; *elp3^{Δ3/Δ4}* mutant larvae; western blots were probed with anti-acetylated tubulin (ac-TUB) or total tubulin (TUB).

(D) In vitro acetylation of IPed BRP (with BRP^{NC82}) from *w¹¹¹⁸* brains with an ELP3-enriched fraction. Western blots were probed with Ac-K and re-probed with BRP^{D2}.

(E and F) Quantification of ELP3-dependent acetylation of tubulin and of BRP normalized to total tubulin or total BRP levels relative to initial acetylation levels (time point "0"). Number of independent repeats is indicated in the bars.

H3 (Figure 7B), but we did not observe ELP3-dependent acetylation of tubulin in wild-type fly lysate, or in lysate prepared from *elp3* null mutant animals (Figures 7C and 7E; data not shown). Thus, although our ELP3 fraction is active, it does not support acetylation of tubulin in vitro. Finally, we tested acetylation of BRP in vitro. We immunoprecipitated BRP from fly heads (see also Figure 8H), incubated these BRP-enriched fractions with Acetyl-CoA and ELP3, and probed western blots with Ac-K (Figure 7D). As shown in Figures 7D and 7F, we find obvious time-dependent acetylation of BRP. These data indicate that ELP3 is sufficient for the acetylation of the active zone-associated protein BRP.

To determine if ELP3 acetylates BRP in vivo, we labeled NMJs with Ac-K. Ac-K labels histones in nuclei (data not shown), microtubules in axons that we marked using the monoclonal antibody Futsch^{22C10} (Figures 8A and 8B), as well as several features in synaptic boutons (Figures 8A and 8C). Furthermore, overexpression of HDAC6 shows a marked reduction in Ac-K that decorates microtubules labeled by Futsch^{22C10}, indicating that the antibodies are specific (Figure 8E). Interestingly, anti-acetylated lysine labeling that overlaps with BRP^{NC82} labeling is much reduced in *elp3* mutants compared to controls (Figures 8C, 8D, 8F, and 8G). The reduction in labeling is specific to active zones because Ac-K labeling overlapping with Futsch^{22C10} is not significantly different in *elp3* mutants compared to controls (Figures 8A, 8B, and 8E). The data suggest that less acetylated lysines are present at active zones in *elp3* mutants.

Next, we immunoprecipitated BRP from control and *elp3* RNAi-expressing pharate adult brains and probed western blots

with Ac-K. BRP immunoprecipitations (IPs) from control animals show an acetylated lysine band that migrates at the same height of BRP, detected with antibodies against the middle domain of BRP, BRP^{D2} (Figures 8H and 7D). This band is largely absent in western blots of IPs from pharate adult brains that express RNAi to *brp*, indicating that the band is specific to BRP and suggesting that at least some BRP is acetylated under basal conditions. Interestingly, in BRP IPs from animals that express RNAi to *elp3*, we are able to clearly detect BRP, but the acetylated lysine band at the height of BRP is largely absent (Figure 8H). These data corroborate the labeling of acetylated lysines at boutons and suggest that ELP3 is necessary to maintain the acetylation status of the active zone-associated protein BRP.

DISCUSSION

In this work we provide evidence that ELP3 acetylates the active zone-associated cytoskeletal-like protein BRP that is increasingly implicated in neuronal diseases (Choi et al., 2010; Zweier et al., 2009). ELP3-mediated BRP acetylation regulates dense body structure, akin to the modification of chromatin structure in the nucleus, and this function is independent of an effect of ELP3 on tubulin acetylation. We suggest that decreased BRP acetylation in *elp3* mutants results in expanded cytoplasmic specializations that capture synaptic vesicles, and our work points to a model where individual release site morphology and function may be controlled by BRP acetylation.

Tubulin Acetylation in the Absence of ELP3

Recent work suggests that besides a role in acetylating histones, ELP3 also acetylates tubulin (Creppe et al., 2009; Solinger et al., 2010); however, several of our observations using different

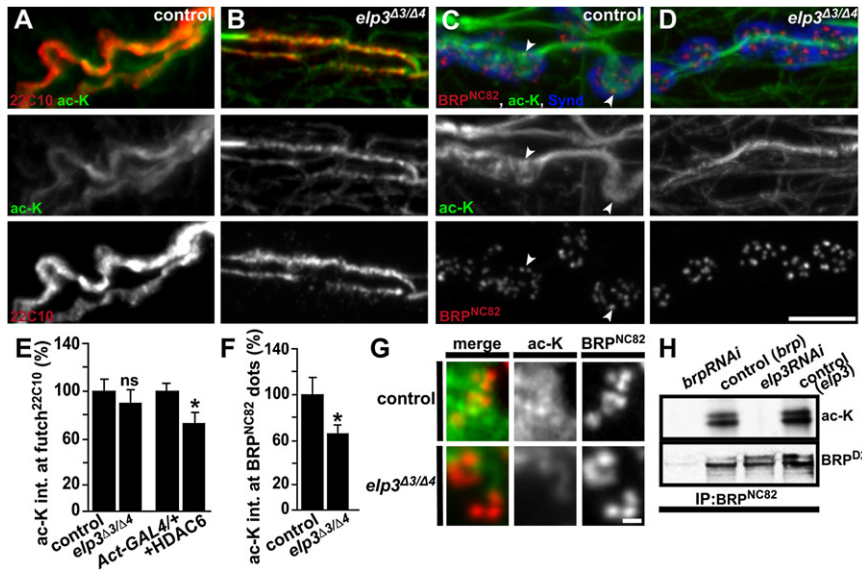


Figure 8. ELP3 Is Necessary to Acetylate BRP

(A–G) Double labeling of NMJs in control *elp3^{ev}* (A, C, and G) and *y,w; elp3^{Δ3/Δ4}* mutant L3 larvae (B, D, and G), stained with Ac-K and Futsch^{22C10}, a microtubule-associated protein (A and B), or BRP^{NC82} (C, D, and G) and mean Ac-K intensity within the area marked with Futsch^{22C10} (E) or BRP^{NC82} (F) relative to controls from eight to ten NMJs from more than four larvae. Error bars, SEM. t test, **p* < 0.05. Scale bars, 5 μm (A–D in D) and 0.5 μm (G). ns, not significant.

(H) Western blot of IPed BRP (using BRP^{NC82}) from *brp-RNAi* (*w DCR2; UAS-brpRNAi/nsyb-Gal4*), control (*w DCR2; nsyb-Gal4/+*), and *elp3-RNAi* (*w; UAS-elp3RNAi^{CS8/+}; da-Gal4/+*), and its control (*w; da-Gal4/+*) pupal brains were probed with Ac-K or with BRP^{D2}.

species and cell types indicate that microtubules can be acetylated by a mechanism that does not involve ELP3. Similar to our findings, in human neuroblastoma cells or in mouse embryonic fibroblasts, ELP1 knockdown results in a profound reduction of ELP3 expression, but also this condition did not affect the levels of acetylated tubulin (Cheishvili et al., 2011). Although in vitro our ELP3 fraction was not able to increase tubulin acetylation, when the protein is overexpressed in N2a cells or in *Drosophila* motor neurons, we find a mild increase in acetylation of tubulin (data not shown), but our work shows that this activity is limited outside of overexpression conditions. It is interesting that an alternative GNAT domain protein, MEC-17, was shown to acetylate tubulin in different systems, including nematodes, zebrafish, and ciliates (Akella et al., 2010); in addition, an acetyltransferase complex, ARD1-NAT1, that can acetylate tubulin in vitro has been found associated with tubulin in developing dendrites of cultured hippocampal neurons and was shown to regulate dendritic outgrowth in vitro (Ohkawa et al., 2008). Thus, alternative tubulin acetyltransferases that regulate neuronal morphology have been identified.

ELP3 Is a BRP Acetyltransferase and Controls Active Zone Morphology

In a search of alternative cytoplasmic ELP3 targets, we identified BRP, a large cytoskeletal-like protein that decorates the active zone where synaptic vesicles fuse with the membrane. We provide several lines of evidence that ELP3 acts to acetylate BRP at the *Drosophila* NMJ. First, ELP3 is present at NMJ boutons, localizing the enzyme in close proximity to BRP. Second, acetylated lysine levels that overlap with BRP^{NC82} labeling at the NMJ are reduced in *elp3* mutants. Similarly, BRP-associated acetylated lysine levels detected by western blotting are reduced in *elp3* mutants. Third, immunoprecipitated BRP is efficiently acetylated by purified ELP3 in vitro. Without excluding other substrates, our data indicate that ELP3 is necessary and sufficient to acetylate BRP. BRP is indeed an excellent candidate to undergo this modification as it contains numerous coiled-

coil motifs that were recently shown to be ideal acetylation substrates (Choudhary et al., 2009).

Individual BRP strands organize into parasol-like structures, with their N termini facing the plasma membrane, contacting calcium channels, and their C termini extending into the cytoplasm capturing synaptic vesicles (Fouquet et al., 2009; Hallermann et al., 2010b; Jiao et al., 2010). While mutations that affect BRP transport to synapses or assembly of T bars at active zones exist, our data indicate that these processes are not affected in *elp3* mutants. Unlike *SRPK79D* mutants (Johnson et al., 2009; Nieratschker et al., 2009), BRP^{NC82} does not accumulate in *elp3* mutant motor neurons (data not shown), suggesting normal axonal transport. In addition, in contrast to *rab3* mutants (Graf et al., 2009), the number of T bars per synaptic area is not different in controls and *elp3* mutants.

Our analyses also identified a postsynaptic role for *elp3* in regulating glutamate receptor subunit IIA abundance in muscles at NMJs and, thus, mEJC amplitude; however, unlike ELP3's neuronal function, we show that this role of ELP3 is not critical for viability, as muscular expression of the protein does not rescue *elp3*-associated lethality. Nonetheless, by regulating postsynaptic receptor field size, ELP3 may also modulate neuronal communication. We present evidence that this defect is regulated in muscle cells independently of the presynaptic role of ELP3.

Using different independent methodologies, we provide evidence that ELP3 regulates presynaptic neurotransmitter release efficiency. We show that during a short high-frequency stimulation train, *elp3* mutants show a stronger increase in SpH fluorescence than controls. Furthermore, mutants release more quanta than controls during a short 100 Hz stimulation train, and this is also true in mutant animals that express hELP3 in muscles and, thus, do not display increased GluRIIA levels. While these data are consistent with a larger pool of readily releasable vesicles in the mutants, a larger Pr in *elp3* mutants may also contribute to increased release. Given that γDGG only partially prevents postsynaptic receptor saturation

at the NMJ, our estimates of Pr in high calcium based on fluctuation analysis are less accurate. However, in 5 mM calcium the Pr is invariably high, limiting the difference in Pr between controls and mutants. In addition, an increased Pr but not a larger RRP in *el3* mutants would alter the time course by which neurotransmitters are released during the 500 ms 100 Hz stimulation paradigm, but the total number of released quanta would not be different between *el3* mutants and controls, particularly in mutants where the postsynaptic defects are rescued, and differences in receptor abundance are eliminated. Thus, while not excluding an effect of ELP3 on the Pr in high calcium, our data are most consistent with an increased RRP in *el3* mutants.

Our work suggests a model where acetylation of BRP reorganizes the cytoplasmic tentacles such that deacetylation leads to more extensive spreading of the strands, possibly by altering electrostatic interactions, similar to the regulation of chromatin structure by histone acetylation (Shogren-Knaak et al., 2006). At active zones, we speculate that this function regulates vesicle capturing by the C-terminal end of BRP (Hallermann et al., 2010b), and transport of vesicles at dense bodies. We present evidence that the defect in *el3* mutants results in a larger pool of synaptic vesicles that is ready for immediate release, potentially in part by improved vesicle tethering at T bars. Although the mechanisms that regulate local ELP3 activity levels at the synapse (but also those that regulate ELP3 activity in the nucleus) remain elusive, it will be interesting to identify signaling pathways that activate ELP3 enzymatic function. The local regulation of ELP3 may enable single active zones to control neurotransmitter release and may have important implications for synaptic transmission regulation in a number of neurological diseases, including ALS and familial dysautonomia (Simpson et al., 2009; Slaugenhaupt and Gusella, 2002).

EXPERIMENTAL PROCEDURES

Animals and Cells

All *Drosophila* lines were kept on cornmeal and molasses medium. For experiments L3 larvae were grown on black currant juice agar plates with fresh yeast paste. GAL4 > UAS-expressing larvae and controls were raised at 28°C (rescue and HDAC6) or at 25°C (CAC-GFP, GCaMP3, SpH, and RNAi). *el3⁴³*, *el3⁴⁴*, and *el3⁴⁵* mutants and *el3^{rev}* controls were created by *P* element dysgenesis using *y¹w^{67c23}*, *P(SUP or-P)el3^{KG02386}*.

Adult zebrafish (AB) and embryos were maintained and staged as described (Westerfield, 2003). The *el3* ATG-morpholino is from Gene Tools, LLC (Corvallis, OR, USA): 5'-TGGCTTCCCATCTTAGACACAATC-3' (ATG-MO); reverse control 5'-CTAACACAGATTCTACCTTTCCGGT-3' (Ctr-MO). A total of 2 μM tubastatin A or DMSO treatment was started at 6 hpf. Axonal defects were evaluated at 30 hpf (Lemmens et al., 2007).

N2a, HEK293T, and NSC34 cells were grown under standard conditions, and cortical neurons, motor neurons, and glial feeder layer cells were prepared as described (Vandenbergh et al., 1998).

Constructs

UAS-help3 was created by cloning the human *el3* cDNA (OriGene) into the EcoRI site of pUAST-attB. Genomic *GFP-el3⁺* and *el3⁺-GFP* constructs were generated using recombineering in *attB*-P(acman)-Ap^R (Venken et al., 2006, 2008) using BAC RP98-28K16. These constructs were inserted in VK31 (62E1) and VK01 (59D3) sites using phiC31-mediated integration (GenetiVision, Houston).

For protein expression, *Drosophila el3* cDNA (RE35395, BDGP) was cloned into a pDEST14 expression vector using Gateway technology (Invitrogen) and includes an N-terminal 6xHis tag.

Biochemistry

Drosophila, zebrafish, and cellular extracts for westerns were prepared using standard procedures and probed with the antibodies listed below.

IP of BRP from pupal or adult brain extracts was performed using BRP^{NC82} diluted 1:5 (Developmental Studies Hybridoma Bank, Iowa City, IA, USA) and G protein-coupled magnetic beads (BioLabs) using *Drosophila* head lysate (Supplemental Experimental Procedures), and IPed protein was either used for acetylation assays or for westerns.

Drosophila ELP3 was expressed in *E. coli* Rosetta (DE3) pLysS cells (Promega). In vitro acetylation was performed by incubating purified ELP3 with substrate in acetylation buffer (50 mM Tris-HCl [pH 8.0], 0.1 mM EDTA, 1 mM DTT, 10 mM Na-butyrate, 10% glycerol) and 20 mM acetyl CoA (Sigma-Aldrich) at 25°C (Chen and Greene, 2005). Substrates used were purified Histone H3 (Westburg) and beads with BRP or *Drosophila* head protein lysate (for acetylation of tubulin).

Western blotting antibodies were: 1:500 anti-Acetylated lysine (Ac-K) (rabbit, AB80178; abCAM); 1:1,000 anti-BRP^N and 1:1,000 anti-BRP^{D2} (Fouquet et al., 2009); 1:1,000 anti-neuronal synaptobrevin (nSYB^{R29}) and 1:500 anti-Histone H3 (9715L; Cell Signaling); 1:10,000 anti-Acetylated α -Tubulin (6-11-B-1; Sigma-Aldrich); 1:1,000 anti- α -Tubulin (B5-12; Sigma-Aldrich); 1:5,000 anti- β -actin (A5441; Sigma-Aldrich); 1:1,000 anti-BRP^{NC82} (Developmental Studies Hybridoma Bank); 1:5,000 anti-GAPDH (4300; Ambion); and 1:1,000 HRP-coupled secondary antibodies (Jackson ImmunoResearch). Blots were developed with Western Lightning ECL (PerkinElmer).

Fluorescence Microscopy

Drosophila third-instar larvae were prepared as described (Uytterhoeven et al., 2011). Primary antibodies were: 1:100 BRP^{NC82}, 1:100 Futsch^{22C10}, 1:25 anti-GLURIIIA^{8B4D2}, 1:50 Anti-DLG^{4F3}, and 1:2 anti-FASII^{1D4} (all from Developmental Studies Hybridoma Bank); 1:50 anti-CSF⁴⁹ (Zinsmaier et al., 1994); 1:1,000 anti-HRP (Jackson ImmunoResearch); 1:300 anti-BRP^N and 1:1,000 anti-Liprin (Owald et al., 2010); 1:200 anti-DYN (Hudy1; Millipore); 1:500 anti-nSYB^{R29} and 1:200 anti-Syndapin (both gifts from H. Bellen, BCM); 1:500 anti-GLURIII (Marrus et al., 2004); 1:10,000 anti-vGLUT (Daniels et al., 2004) (both gifts from A. Di Antonio, Washington University); 1:200 anti-Acetylated Lysines (Ac-K) (ab80178; abCAM); 1:1,000 anti-Acetylated α -Tubulin (6-11-B-1; Sigma-Aldrich); 1:500 anti-GFP (rabbit IgG fraction; Invitrogen) to detect GFP-ELP3, ELP3-GFP, and Cac-GFP signals; and 1:1,000 secondary Alexa 488, 555, or 645-conjugated antibodies (Invitrogen). TOTO3 (Invitrogen) was used to label DNA and was used at 1:500 in PBS prior to mounting samples. NMJs were imaged through 63 \times 1.4 NA oil lens on a Zeiss 510 Meta confocal microscope, and mean fluorescence intensities of labeling per bouton and background were measured using ImageJ as described (Khuong et al., 2010; Uytterhoeven et al., 2011). The number of BRP spots per area was counted following automated thresholding in ImageJ and calculated from measurements of ≥ 6 type 1b boutons per NMJ on M6/7 in segments A2/3.

Electron Microscopy

L3 larvae were dissected in HL-3 and prepared for TEM, and bouton profiles in 50 nm sections from M6/7 in segment A2 were visualized on a JEOL TEM100 (Uytterhoeven et al., 2011). At least 17 images from 3 animals were analyzed. Serial-tilt EM was performed on 300 nm sections, and micrographs were recorded from -60° to 60° at 2° intervals. 3D reconstructions were generated in IMOD (Uytterhoeven et al., 2011).

Electrophysiology

Recordings from L3 M6 in segment A2/3 were performed on an Axoclamp 900A amplifier, filtered at 1 kHz (400 Hz for minis), and stored in pClamp 10.3 in modified HL-3: 110 mM NaCl, 5 mM KCl, 10 mM NaHCO₃, 5 mM HEPES, 30 mM sucrose, 5 mM trehalose, 10 mM MgCl₂, CaCl₂ (as indicated) [pH 7.2], using a holding potential of -70 mV (Uytterhoeven et al., 2011). Where indicated, 0.5 μM TTX (for mini recordings, not in Figures S6E and S6F) or 10 mM γ -DGG (Tocris Bioscience) was added (Pawlu et al., 2004) for 10 min prior to recordings.

Fluctuation analysis was performed as described (Weyhersmüller et al., 2011).

The RRP size from cumulative EJC plots was determined as described (Weyhersmüller et al., 2011; Hallermann et al., 2010a) except that 50 stimuli were delivered at 100 Hz. EJC amplitudes were measured from peak to the baseline (lowest level) immediately before the onset of the EJC. Trend lines were calculated between the 30th and 50th stimulation point and back extrapolated to time zero.

Time-Lapse Imaging

GCaMP3 and SpH were expressed with *nSyb-Gal4* in *elp3^{ev}* and *elp3* mutants, and imaging was performed as described (Hendel et al., 2008; Uytterhoeven et al., 2011).

SUPPLEMENTAL INFORMATION

Supplemental Information includes six figures and Supplemental Experimental Procedures and can be found with this article online at doi:10.1016/j.neuron.2011.10.010.

ACKNOWLEDGMENTS

We thank the Vienna *Drosophila* RNAi Center, the Bloomington and Harvard *Drosophila* stock centers, and the Developmental Studies Hybridoma bank as well as Hugo Bellen and Aaron DiAntonio for reagents. We especially thank Ron Habets as well as Sebastian Munck, Pieter Baatsen, and Jan Slabbaert, and other members of the P.V., W.R., and W.V. labs for help and comments. Support was provided by a Marie Curie Excellence grant (MEXT-CT-2006-042267), an ERC Starting Grant (260678), FWO Grants G094011, G095511, G074709, and G025909, the Research Fund KU Leuven: BOF-OT and GOA 11/014, Interuniversity attraction Poles (IUAP) program P6/43 of the Belgian Federal Science Policy Office, the Motor Neuron Disease Association UK (6046), The European Community's Health Seventh Framework Programme (FP7/2007-2013; 259867), a Methusalem grant of the Flemish Government, the Francqui Foundation, the Hercules Foundation (project AKUL/09/037), and VIB. W.V. is supported by an FWO postdoctoral grant, M.F. by an IWT predoctoral grant, L.E.J. by a predoctoral VIB fellowship, and W.R. by a E. von Behring Chair for Neuromuscular and Neurodegenerative Disorders.

Accepted: October 5, 2011

Published: December 7, 2011

REFERENCES

- AKella, J.S., Wloga, D., Kim, J., Starostina, N.G., Lyons-Abbott, S., Morrisette, N.S., Dougan, S.T., Kipreos, E.T., and Gaertig, J. (2010). MEC-17 is an alpha-tubulin acetyltransferase. *Nature* **467**, 218–222.
- Cheishvili, D., Maayan, C., Cohen-Kupiec, R., Lefler, S., Weil, M., Ast, G., and Razin, A. (2011). IKAP/Elp1 involvement in cytoskeleton regulation and implication for familial dysautonomia. *Hum. Mol. Genet.* **20**, 1585–1594.
- Chen, L.F., and Greene, W.C. (2005). Assessing acetylation of NF-kappaB. *Methods* **36**, 368–375.
- Choi, J.K., Jeon, Y.C., Lee, D.W., Oh, J.M., Lee, H.P., Jeong, B.H., Carp, R.I., Koh, Y.H., and Kim, Y.S. (2010). A *Drosophila* model of GSS syndrome suggests defects in active zones are responsible for pathogenesis of GSS syndrome. *Hum. Mol. Genet.* **19**, 4474–4489.
- Choudhary, C., Kumar, C., Gnad, F., Nielsen, M.L., Rehman, M., Walther, T.C., Olsen, J.V., and Mann, M. (2009). Lysine acetylation targets protein complexes and co-regulates major cellular functions. *Science* **325**, 834–840.
- Creppe, C., Malinowskaya, L., Volvert, M.L., Gillard, M., Close, P., Malaise, O., Laguesse, S., Cornez, I., Rahmouni, S., Ormenese, S., et al. (2009). Elongator controls the migration and differentiation of cortical neurons through acetylation of alpha-tubulin. *Cell* **136**, 551–564.
- Daniels, R.W., Collins, C.A., Gelfand, M.V., Dant, J., Brooks, E.S., Krantz, D.E., and DiAntonio, A. (2004). Increased expression of the *Drosophila* vesicular glutamate transporter leads to excess glutamate release and a compensatory decrease in quantal content. *J. Neurosci.* **24**, 10466–10474.
- DiAntonio, A., Petersen, S.A., Heckmann, M., and Goodman, C.S. (1999). Glutamate receptor expression regulates quantal size and quantal content at the *Drosophila* neuromuscular junction. *J. Neurosci.* **19**, 3023–3032.
- Foster, K.A., and Regehr, W.G. (2004). Variance-mean analysis in the presence of a rapid antagonist indicates vesicle depletion underlies depression at the climbing fiber synapse. *Neuron* **43**, 119–131.
- Fouquet, W., Oswald, D., Wichmann, C., Mertel, S., Depner, H., Dyba, M., Hallermann, S., Kittel, R.J., Eimer, S., and Sigrist, S.J. (2009). Maturation of active zone assembly by *Drosophila* Bruchpilot. *J. Cell Biol.* **186**, 129–145.
- Graf, E.R., Daniels, R.W., Burgess, R.W., Schwarz, T.L., and DiAntonio, A. (2009). Rab3 dynamically controls protein composition at active zones. *Neuron* **64**, 663–677.
- Hallermann, S., Heckmann, M., and Kittel, R.J. (2010a). Mechanisms of short-term plasticity at neuromuscular active zones of *Drosophila*. *HFSP J.* **4**, 72–84.
- Hallermann, S., Kittel, R.J., Wichmann, C., Weyhersmüller, A., Fouquet, W., Mertel, S., Oswald, D., Eimer, S., Depner, H., Schwärzel, M., et al. (2010b). Naked dense bodies provoke depression. *J. Neurosci.* **30**, 14340–14345.
- Han, Q., Lu, J., Duan, J., Su, D., Hou, X., Li, F., Wang, X., and Huang, B. (2008). Gcn5- and Elp3-induced histone H3 acetylation regulates hsp70 gene transcription in yeast. *Biochem. J.* **409**, 779–788.
- Haucke, V., Neher, E., and Sigrist, S.J. (2011). Protein scaffolds in the coupling of synaptic exocytosis and endocytosis. *Nat. Rev. Neurosci.* **12**, 127–138.
- Hendel, T., Mank, M., Schnell, B., Griesbeck, O., Borst, A., and Reiff, D.F. (2008). Fluorescence changes of genetic calcium indicators and OGB-1 correlated with neural activity and calcium in vivo and in vitro. *J. Neurosci.* **28**, 7399–7411.
- Hida, Y., and Ohtsuka, T. (2010). CAST and ELKS proteins: structural and functional determinants of the presynaptic active zone. *J. Biochem.* **148**, 131–137.
- Hubbert, C., Guardiola, A., Shao, R., Kawaguchi, Y., Ito, A., Nixon, A., Yoshida, M., Wang, X.F., and Yao, T.P. (2002). HDAC6 is a microtubule-associated deacetylase. *Nature* **417**, 455–458.
- Jiao, W., Masich, S., Franzén, O., and Shupliakov, O. (2010). Two pools of vesicles associated with the presynaptic cytosolic projection in *Drosophila* neuromuscular junctions. *J. Struct. Biol.* **172**, 389–394.
- Johnson, E.L., 3rd, Fetter, R.D., and Davis, G.W. (2009). Negative regulation of active zone assembly by a newly identified SR protein kinase. *PLoS Biol.* **7**, e1000193.
- Khuong, T.M., Habets, R.L., Slabbaert, J.R., and Verstreken, P. (2010). WASP is activated by phosphatidylinositol-4,5-bisphosphate to restrict synapse growth in a pathway parallel to bone morphogenetic protein signaling. *Proc. Natl. Acad. Sci. USA* **107**, 17379–17384.
- Kittel, R.J., Wichmann, C., Rasse, T.M., Fouquet, W., Schmidt, M., Schmid, A., Wagh, D.A., Pawlu, C., Kellner, R.R., Willig, K.I., et al. (2006). Bruchpilot promotes active zone assembly, Ca²⁺ channel clustering, and vesicle release. *Science* **312**, 1051–1054.
- Lemmens, R., Van Hoecke, A., Hersmus, N., Geelen, V., D'Hollander, I., Thijs, V., Van Den Bosch, L., Carmeliet, P., and Robberecht, W. (2007). Overexpression of mutant superoxide dismutase 1 causes a motor axonopathy in the zebrafish. *Hum. Mol. Genet.* **16**, 2359–2365.
- Marrus, S.B., Portman, S.L., Allen, M.J., Moffat, K.G., and DiAntonio, A. (2004). Differential localization of glutamate receptor subunits at the *Drosophila* neuromuscular junction. *J. Neurosci.* **24**, 1406–1415.
- Miesenböck, G., De Angelis, D.A., and Rothman, J.E. (1998). Visualizing secretion and synaptic transmission with pH-sensitive green fluorescent proteins. *Nature* **394**, 192–195.
- Nicoll, R.A., and Schmitz, D. (2005). Synaptic plasticity at hippocampal mossy fibre synapses. *Nat. Rev. Neurosci.* **6**, 863–876.
- Nieratschker, V., Schubert, A., Jauch, M., Bock, N., Bucher, D., Dippacher, S., Krohne, G., Asan, E., Buchner, S., and Buchner, E. (2009). Bruchpilot in ribbon-like axonal agglomerates, behavioral defects, and early death in SRPK79D kinase mutants of *Drosophila*. *PLoS Genet.* **5**, e1000700.

- Ohkawa, N., Sugisaki, S., Tokunaga, E., Fujitani, K., Hayasaka, T., Setou, M., and Inokuchi, K. (2008). N-acetyltransferase ARD1-NAT1 regulates neuronal dendritic development. *Genes Cells* 13, 1171–1183.
- Otero, G., Fellows, J., Li, Y., de Bizemont, T., Dirac, A.M., Gustafsson, C.M., Erdjument-Bromage, H., Tempst, P., and Svejstrup, J.Q. (1999). Elongator, a multisubunit component of a novel RNA polymerase II holoenzyme for transcriptional elongation. *Mol. Cell* 3, 109–118.
- Owald, D., Fouquet, W., Schmidt, M., Wichmann, C., Mertel, S., Depner, H., Christiansen, F., Zube, C., Quentin, C., Körner, J., et al. (2010). A Syd-1 homologue regulates pre- and postsynaptic maturation in *Drosophila*. *J. Cell Biol.* 188, 565–579.
- Pawlu, C., DiAntonio, A., and Heckmann, M. (2004). Postfusional control of quantal current shape. *Neuron* 42, 607–618.
- Peled, E.S., and Isacoff, E.Y. (2011). Optical quantal analysis of synaptic transmission in wild-type and rab3-mutant *Drosophila* motor axons. *Nat. Neurosci.* 14, 519–526.
- Pelkey, K.A., and McBain, C.J. (2007). Differential regulation at functionally divergent release sites along a common axon. *Curr. Opin. Neurobiol.* 17, 366–373.
- Pelkey, K.A., Topolnik, L., Lacaille, J.C., and McBain, C.J. (2006). Compartmentalized Ca²⁺ channel regulation at divergent mossy-fiber release sites underlies target cell-dependent plasticity. *Neuron* 52, 497–510.
- Petersen, S.A., Fetter, R.D., Noordermeer, J.N., Goodman, C.S., and DiAntonio, A. (1997). Genetic analysis of glutamate receptors in *Drosophila* reveals a retrograde signal regulating presynaptic transmitter release. *Neuron* 19, 1237–1248.
- Schmid, A., Hallermann, S., Kittel, R.J., Khorramshahi, O., Frölich, A.M., Quentin, C., Rasse, T.M., Mertel, S., Heckmann, M., and Sigrist, S.J. (2008). Activity-dependent site-specific changes of glutamate receptor composition in vivo. *Nat. Neurosci.* 11, 659–666.
- Shogren-Knaak, M., Ishii, H., Sun, J.M., Pazin, M.J., Davie, J.R., and Peterson, C.L. (2006). Histone H4-K16 acetylation controls chromatin structure and protein interactions. *Science* 311, 844–847.
- Simpson, C.L., Lemmens, R., Miskiewicz, K., Broom, W.J., Hansen, V.K., van Vught, P.W., Landers, J.E., Sapp, P., Van Den Bosch, L., Knight, J., et al. (2009). Variants of the elongator protein 3 (ELP3) gene are associated with motor neuron degeneration. *Hum. Mol. Genet.* 18, 472–481.
- Slaugenhaupt, S.A., and Gusella, J.F. (2002). Familial dysautonomia. *Curr. Opin. Genet. Dev.* 12, 307–311.
- Solinger, J.A., Paolinelli, R., Klöss, H., Scorza, F.B., Marchesi, S., Sauder, U., Mitsushima, D., Capuani, F., Stürzenbaum, S.R., and Cassata, G. (2010). The *Caenorhabditis elegans* Elongator complex regulates neuronal alpha-tubulin acetylation. *PLoS Genet.* 6, e1000820.
- Tian, L., Hires, S.A., Mao, T., Huber, D., Chiappe, M.E., Chalasani, S.H., Petreanu, L., Akerboom, J., McKinney, S.A., Schreiter, E.R., et al. (2009). Imaging neural activity in worms, flies and mice with improved GCaMP calcium indicators. *Nat. Methods* 6, 875–881.
- Uytterhoeven, V., Kuenen, S., Kasprovicz, J., Miskiewicz, K., and Verstreken, P. (2011). Loss of skywalker reveals synaptic endosomes as sorting stations for synaptic vesicle proteins. *Cell* 145, 117–132.
- Vandenbergh, W., Van Den Bosch, L., and Robberecht, W. (1998). Glial cells potentiate kainate-induced neuronal death in a motoneuron-enriched spinal coculture system. *Brain Res.* 807, 1–10.
- Venken, K.J., He, Y., Hoskins, R.A., and Bellen, H.J. (2006). P[acman]: a BAC transgenic platform for targeted insertion of large DNA fragments in *D. melanogaster*. *Science* 314, 1747–1751.
- Venken, K.J., Kasprovicz, J., Kuenen, S., Yan, J., Hassan, B.A., and Verstreken, P. (2008). Recombineering-mediated tagging of *Drosophila* genomic constructs for in vivo localization and acute protein inactivation. *Nucleic Acids Res.* 36, e114.
- Versées, W., De Groeve, S., and Van Lijsebettens, M. (2010). Elongator, a conserved multitasking complex? *Mol. Microbiol.* 76, 1065–1069.
- Walia, H., Chen, H.Y., Sun, J.M., Holth, L.T., and Davie, J.R. (1998). Histone acetylation is required to maintain the unfolded nucleosome structure associated with transcribing DNA. *J. Biol. Chem.* 273, 14516–14522.
- Walker, J., Kwon, S.Y., Badenhorst, P., East, P., McNeill, H., and Svejstrup, J.Q. (2011). Role of elongator subunit Elp3 in *Drosophila melanogaster* larval development and immunity. *Genetics* 187, 1067–1075.
- Westerfield, M. (2003). *The Zebrafish Book* (Eugene, OR: The University of Oregon Press).
- Weyhersmüller, A., Hallermann, S., Wagner, N., and Eilers, J. (2011). Rapid active zone remodeling during synaptic plasticity. *J. Neurosci.* 31, 6041–6052.
- Winkler, G.S., Kristjuhan, A., Erdjument-Bromage, H., Tempst, P., and Svejstrup, J.Q. (2002). Elongator is a histone H3 and H4 acetyltransferase important for normal histone acetylation levels in vivo. *Proc. Natl. Acad. Sci. USA* 99, 3517–3522.
- Zhai, R.G., and Bellen, H.J. (2004). The architecture of the active zone in the presynaptic nerve terminal. *Physiology (Bethesda)* 19, 262–270.
- Zinsmaier, K.E., Eberle, K.K., Buchner, E., Walter, N., and Benzer, S. (1994). Paralysis and early death in cysteine string protein mutants of *Drosophila*. *Science* 263, 977–980.
- Zweier, C., de Jong, E.K., Zweier, M., Orrico, A., Ousager, L.B., Collins, A.L., Bijlsma, E.K., Oortveld, M.A., Ekici, A.B., Reis, A., et al. (2009). CNTNAP2 and NRXN1 are mutated in autosomal-recessive Pitt-Hopkins-like mental retardation and determine the level of a common synaptic protein in *Drosophila*. *Am. J. Hum. Genet.* 85, 655–666.